Materials Today Communications 26 (2021) 102118

Contents lists available at ScienceDirect

Materials Today Communications

journal homepage: www.elsevier.com/locate/mtcomm

A DFT study on stability and electronic structure of AlN nanotubes

İskender Muz [a,*], Hasan Kurban [b,c], Mustafa Kurban [d,*]

[a] Department of Mathematics and Science Education, Nevşehir Hacı Bektas Veli University, 50300, Nevşehir, Turkey
[b] Computer Science Department, Indiana University, Bloomington, 47405, IN, USA
[c] Computer Engineering Department, Siirt University, 56100, Siirt, Turkey
[d] Department of Electrical and Electronics Engineering, Kırşehir Ahi Evran University, 40100, Kırşehir, Turkey

ARTICLE INFO

Keywords:
Aluminum nitride
Nanotube
Segregation phenomena
Energy gap
DFT

ABSTRACT

Structural, energetic, electronic, reactivity and stability properties of armchair (3,3), (4,4), (5,5), (6,6), (7,7), (8,8), (9,9) and (10,10) aluminum nitride nanotubes (AlNNTs) with different diameter have been probed using density functional theory (DFT) in terms of Moreover, the chemical reactivity characteristics of AlNNTs have performed via some of the quantum molecular descriptors. Our results also indicate that the increasing diameter of AlNNTs gives rise to notable changes in the electronic structure of the AlNNTs. Moreover, results for UV/vis spectra of AlNNTs indicate that the maximum wavelength absorption lie in the range 188−194 nm. The number Al-N bonds and segregation phenomena of Al and N atoms in the AlNNTs have been investigated to better understand the stability of AlNNTs. Besides, the energy gap and chemical hardness enhance with increase diameter of AlNNTs, thus resulting in a rise in the stability, while the AlNNTs with smaller can be considered as a candidate for the adsorption of gas molecules and drugs for nano-electronic applications.

1. Introduction

Carbon nanotubes (CNTs) have used in distinct applications as an electrode for oxygen reduction and supercapacitors [1,2], a molecular junction to enhance electron transport ability of electronic devices [3], an anode for lithium-ion battery [4], a delivery system for the anticancer drugs [5,6], gas sensor [7], light-emitting diode [8] and so on due to their intriguing and tunable properties. However, some obstacles such as the non-ideal structure bringing about relatively high resistivity, the large number of thermal defects and chirality-dependent electronic characteristics, make them difficult to be applied in semiconductor devices. To overcome these difficulties, recently, inorganic nanotubes including B, N, Al, Si, Ga, and Ge atoms have been designed both experimentally and theoretically. Among them, most importantly, the aluminum nitride nanotubes (AlNNTs), which were experimentally obtained in the range of 30–80 nm [9], have been researched use in some important fields such as H_2 storage, battery, sensor, etc. [10–12]. It is found that AlNNTs have some advantages over CNTs. For example, AlNNTs as an anode material provide greater cell voltage than CNTs for Li-ion batteries [11]. AlNNTs also are effective for CO adsorption [13, 14] and elimination of C_4H_6 toxic molecule from the environment [15] because of their huge polarity ability enabling noticeably higher reactivity than CNTs.

Nanostructured materials have unique physical and chemical properties according to a change in their size and morphology due to quantum size effects [16–19]. In this perspective, we have carried out, for the first time, systematic research on AlNNTs with different diameters which may considerably modify the electronic properties of them. Therefore, diverse structural and electronic parameters such as the density of states (DOS), orbital energies, energy gap (E_g), binding energy (E_b), the vertical ionization potential and vertical electron affinity (VIP and VEA), point group symmetry, total energy (E_T), the lowest vibrational frequency, chemical hardness (η), electrophilicity index, and maximum amount of electronic charge index (ΔN_{tot}) were calculated using density functional theory (DFT). The UV/visible absorption spectrums of AlNNTs have been also analyzed using time-dependent (TD)-DFT. Moreover, the number of Al-N bonds and order parameter (R) of Al and N atoms in the AlNNTs have analyzed to better understand the stability of AlNNTs. The obtained estimations were discussed in detail.

2. Computational details

In this study, the armchair models of (3,3), (4,4), (5,5), (6,6), (7,7),

* Corresponding authors.
E-mail addresses: iskendermuz@yahoo.com (İ. Muz), mkurbanphys@gmail.com (M. Kurban).

https://doi.org/10.1016/j.mtcomm.2021.102118
Received 24 January 2021; Received in revised form 2 February 2021; Accepted 2 February 2021
Available online 10 February 2021

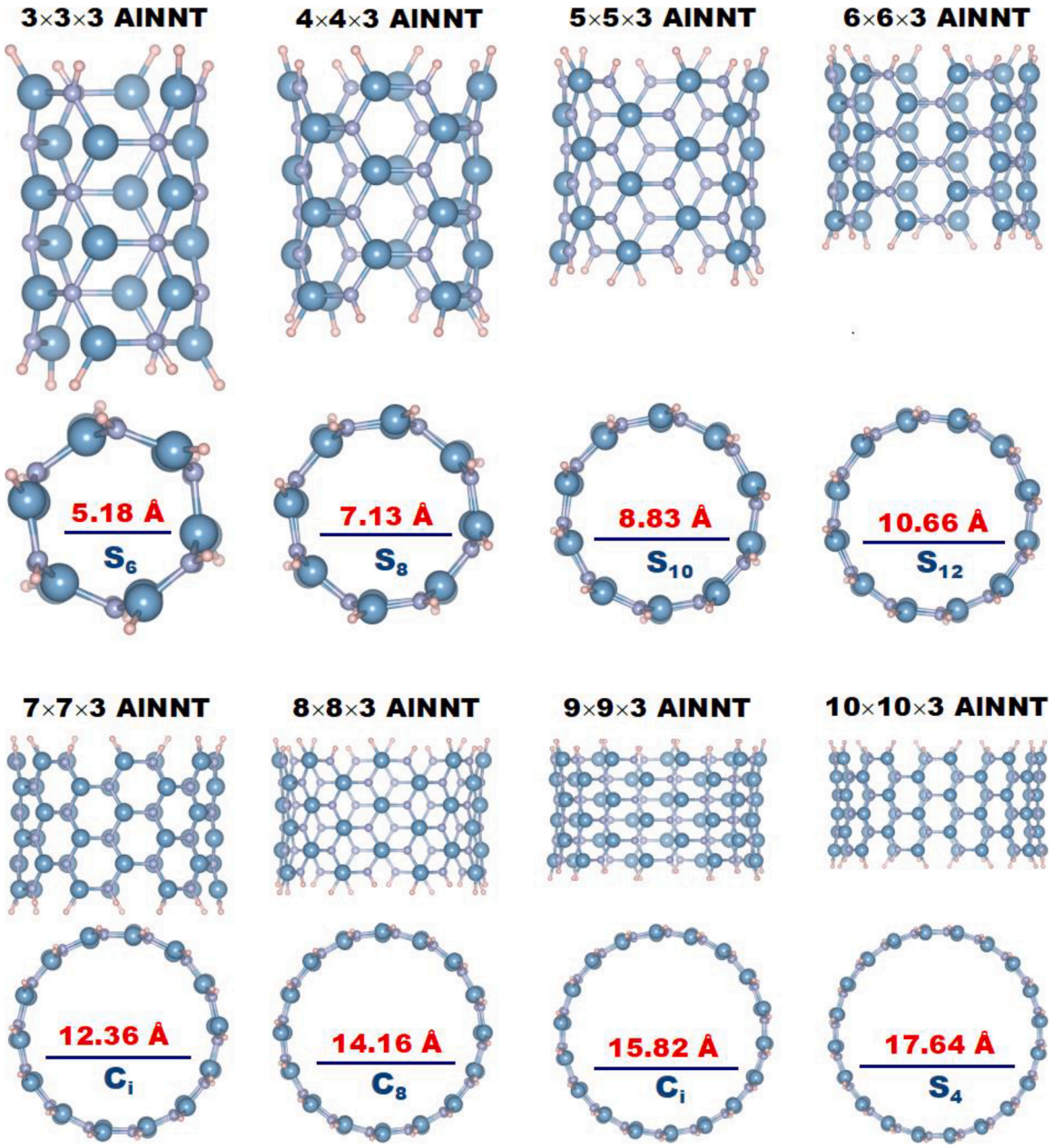

Fig. 1. Side and top views of optimized AlNNT models in different diameters.

(8,8), (9,9) and (10,10) AlN nanotubes (AlNNTs) are chosen. Open ends of the AlNNTs are saturated by hydrogen atoms due to fragment stabilization effect in the system [20]. All calculations was performed by Gaussian 09 program [21] as based on the B3LYP/6-31 G(d) functional [22] for the exchange and the correlation energy together with the empirical dispersion term of Grimme (GD3) [23]. Harmonic vibrational frequencies are also estimated to confirm true minima. The B3LYP functional underestimates excited state energies when compared to CAM-B3LYP and LC-B3LYP functionals. Therefore, the CAM-B3LYP functional [24] is used to calculate absorption spectra of AlNNTs [25–28] based on TD-DFT method.

The binding energy per atom (E_b) are calculated by

$$E_b = [i \times (E(Al) + E(N)) + j \times E(H) - E(AlNNT)]/(2i + j) \quad (1)$$

The vertical ionization potential (VIP) and vertical electron affinity (VEA) were calculated using the following expressions: $[VIP = E^{cation} - E^{neutral}]$ and $[VEA = E^{neutral} - E^{anion}]$. Density of state (DOS) calculations were performed by utilizing GaussSum program [29] to assess the difference in energies of the HOMO − LUMO orbitals (E_{HOMO} and E_{LUMO}). In addition, the Koopman's theorem [30] offers an alternative method to identify the ionization potential and electron affinity through negative of HOMO and LUMO energies (-E_{HOMO} and -E_{LUMO}). Based on this theorem, chemical hardness (η), electrophilicity index (ω) and maximum amount of electronic charge index (ΔN_{tot}) can be determined in terms of orbital energies: $\eta = (I - A)/2$, $\omega = \mu 2/2\eta$ and $\Delta N_{tot} = -\mu/\eta$ [31].

The number of bonds (n_{ij}) [32] is defined by

$$n_{ij} = \sum_{i<j} \delta_{ij} \quad (2)$$

where $\delta_{ij} = \begin{cases} 1, & r_{ij} \le 1.2 r_{ij}^{(0)} \\ 0, & r_{ij} > 1.2 r_{ij}^{(0)} \end{cases}$ $i,j =$ Al or N, r_{ij} is the distance between atom i and j and $r_{ij}^{(0)}$ is a nearest neighbor criterion obtained from the experimental binary data of Al-N interactions [33]. We research the

Table 1
The structural and energetic properties of AlNNT models. (Symm is symmetric structure, E_t is total energy (in Hartree), f is the lowest frequency and E_b is binding energy).

Models	Symm	E_t	f	E_b
3 × 3×3	S_6	−5358.4186	53.18	5.20
4 × 4×3	S_8	−7144.6321	26.89	5.23
5 × 5×3	S_{10}	−8930.8306	17.85	5.24
6 × 6×3	S_{12}	−10717.0233	12.39	5.25
7 × 7×3	C_i	−12503.2126	9.41	5.25
8 × 8×3	C_8	−14289.3995	7.25	5.26
9 × 9×3	C_i	−16075.5849	5.86	5.26
10 × 10 × 3	S_4	−17861.7690	4.41	5.26

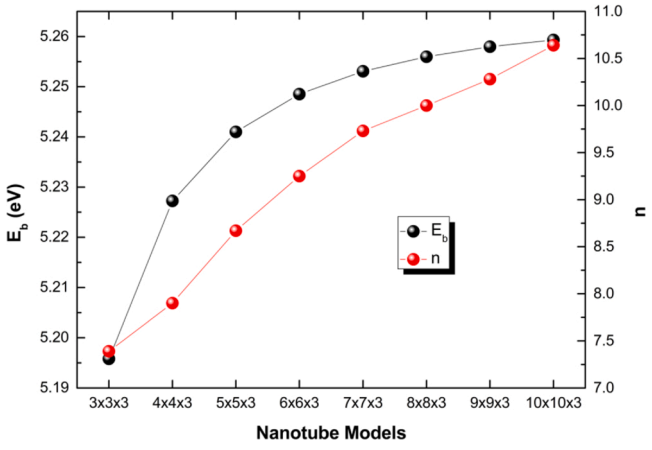

Fig. 2. Binding energy per atom (E_b) and number of bonds (n) of Al-N inteactions of AlNNT models.

atomic distribution of Al and N in AlNNTs by n_{ij}.

We also studied segregation phenomena of the two types of atoms (Al and N) [32–34] with the order parameter (R_{T_i}) to discover the stable structure of AlNNTs with different diameters.

Let n_{T_i} be the number T_i type atoms in the binary AB nanotubes, r_i the distance of the atoms to the coordinate center of the nanotube, then R_{T_i}, the average distance of a type T_i atoms in accordance with the center of a nanotube, is expressed by

$$R_{T_i} = \frac{1}{n_{T_i}} \sum_{i=1}^{n_{T_i}} r_i \tag{3}$$

An ε distance from center of nanotube to a reference point is determined to indicate the position of atoms; if $R_{T_i} < \varepsilon_{min}$ (a "small" value), it means that the T_i type atoms are at the center, and if $R_{T_i} > \varepsilon_{max}$ (a "large" value), it means that the T_i type atoms are at the surface region of NP. If neither is true, *i.e.*, if $\varepsilon_{min} \leq R_{T_i} \leq \varepsilon_{max}$ (a "medium" value), it means a well-mixed NP.

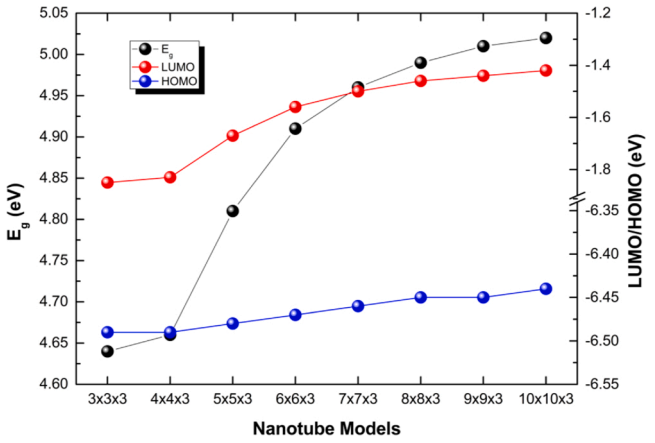

Fig. 3. HOMO, LUMO and HOMO-LUMO energy gap (E_g) of AlNNT models.

3. Results and discussions

We study the structural optimization of armchair (3,3), (4,4), (5,5), (6,6), (7,7), (8,8), (9,9) and (10,10) AlNNTs, in whose cell there are 48, 64, 80, 96, 112, 128, 144 and 160 atoms with various diameters, respectively. The relaxed geometry of AlNNTs is presented in Fig. 1.

The structural properties such as total energy (E_t), point group symmetry (Symm) and lowest frequency (f) is tabulated in Table 1 where we also have listed the binding energy per atom (E_b) of the optimized AlNNTs. There is no negative frequency which indicates the transition state at a saddle-point on the potential energy surface. Note that the lowest vibrational frequencies of AlNNTs are decreased with increasing the size of nanotubes (see Table 1). The point group symmetries of the optimized (3,3), (4,4), (5,5), (6,6), (7,7), (8,8), (9,9) and (10,10) AlNNTs are S_6, S_8, S_{10}, S_{12}, C_i, C_8, C_i, C_4, respectively (see Fig. 1). The Al-N = 1.80 and 1.81 Å bond length between walls are approximately the same for all AlNNTs. In addition, the lengths of the optimized (3,3), (4,4), (5,5), (6,6), (7,7), (8,8), (9,9) and (10,10) AlNNTs are in range of 7.8 and 7.9 Å, and their diameters are 5.18, 7.13, 8.83, 10.66, 12.36, 14.16, 15.82, 17.64 Å, respectively (see Fig. 1). Compared with the pure CNTs [16] and boron nitride nanotubes (BNNTs) [35], the average diameter of AlNNTs is higher than that of the others. In addition, the order of the average diameter of AlNNTs (for $n \times n \times 3$; $n = 3$–8) is found as follows: CNTs < BNNTs < AlNNTs [16].

Fig. 2 shows that the results for the E_b of AlNNTs. The E_b increases with an increase in the AlNNTs diameter. The values in Table 1 imply that the E_b of (3,3) AlNNT is 5.20 eV. The E_b increases with an increase in the AlNNTs diameter, and the highest value is therefore found for (10,10) AlNNT. This also indicates that the stability increases with an increase in the AlNNTs diameter. This trend is compatible with previous our studies showing that the E_b of AlNNTs is lower than that of CNTs [16].

To get more detailed information about the stability, we carry out the number of Al-N binary bonds (n_{AlN}) which is expressed in Eq. (1). There are many parameters to determine the stability of materials, such as

Table 2
The electronic and reactivity properties (in eV) of AlNNT models.

Models	HOMO	LUMO	E_g	VIP	VEA	η	ω	ΔN_{tot}
3 × 3×3	−6.49	−1.85	4.64	7.58	0.79	2.32	20.17	1.80
4 × 4×3	−6.49	−1.83	4.66	7.45	0.87	2.33	20.16	1.79
5 × 5×3	−6.48	−1.67	4.81	7.36	0.81	2.41	19.97	1.69
6 × 6×3	−6.47	−1.56	4.91	7.37	0.78	2.46	19.79	1.64
7 × 7×3	−6.46	−1.50	4.96	7.29	0.78	2.48	19.64	1.60
8 × 8×3	−6.45	−1.46	4.99	7.22	0.79	2.50	19.51	1.59
9 × 9×3	−6.45	−1.44	5.01	7.16	0.81	2.51	19.49	1.57
10 × 10 × 3	−6.44	−1.42	5.02	7.11	0.83	2.51	19.38	1.57

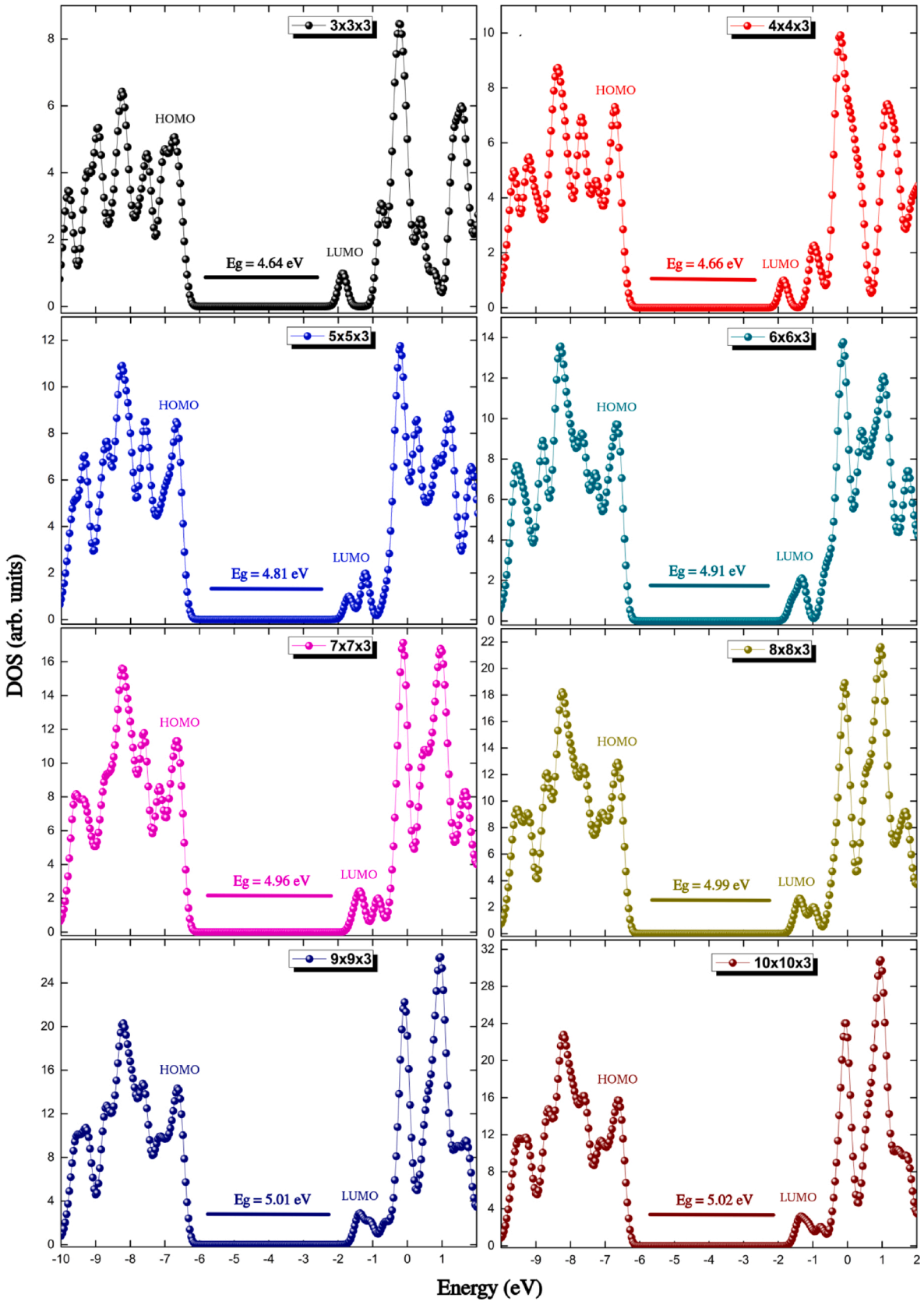

Fig. 4. Density of states (DOS) of AlNNT models.

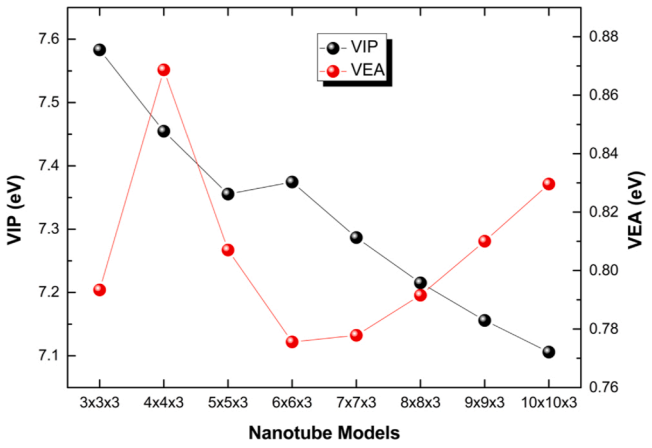

Fig. 5. Vertical ionization potential (VIP) and vertical electron affinity (VEA) of AlNNT models.

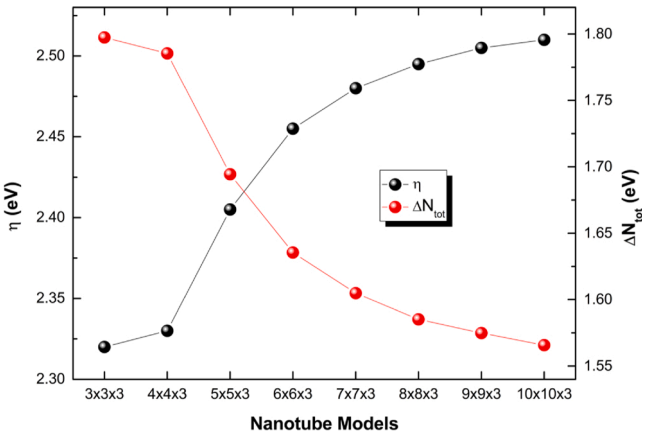

Fig. 6. Chemical hardness (η) and maximum amount of electronic charge index (ΔN_{tot}) of AlNNT models.

larger binding energy and lower vibrational frequency and others. In this part, the order of stability of eight AlNNT models has been correlated in terms of the E_b based on the n_{AlN}. The relationship between the E_b and n_{AlN} is plotted Fig. 2 which shows that an increase in the E_b is proportional to n_{AlN} (the number of Al–N bonds in AlNNTs). Therefore, we can conclude that maximum n_{AlN} corresponds to maximum stability.

The values in Table 2 imply that the energies of HOMO and LUMO levels of (3,3) AlNNT are −6.49 and −1.85 eV, respectively; therefore, the E_g is 4.64 eV. LUMO levels shifted to higher energy with increasing diameter of AlNNTs and the energies of LUMO increase from −1.85 (for (3,3) AlNNT) to −1.42 eV (for (10,10) AlNNT), as seen in Fig. 3. However, the HOMO level remained unchanged by increasing radius of the AlNNTs. Consequently, the E_g shows an increase trend as the diameter of AlNNTs increases. The E_g of (10,10) AlNNT is calculated to be 5.02 eV and this value is bigger than that of the other AlNNTs, indicating electrically a semi-conductive behavior. When it comes to the stability, AlNNT with the biggest diameter has the biggest stability due to its largest HOMO-LUMO gap which is compatible with literature [36,37].

Contrary to BNNTs, AlNNTs are narrower gap semiconductors with the E_g in the range of 4.64–5.02 eV, independently of diameter, chiral and number of walls [38,39]. For example, the E_g of armchair (4,4) AlNNT is calculated to be 4.66 eV in this study, whereas, those of armchair (4,4) BNNT and armchair (5,5) BNNT is reported as 6.29 eV [40] and 6.31 eV [35,41], respectively. On the other hand, the E_g of AlNNTs is larger than that of CNTs [16].

To better understand the sensitivity of the AlNNTs depending on an increase in diameter, we calculated and compared the density of states (DOS) in the energy range −10 to 2 eV, as presented in Fig. 4. We note that notable changes in the DOS are not observed near the Fermi level. However, it can be seen that after an increase in diameter of AlNNTs, a small shift near the conduction band compared to that of the AlNNTs with smaller diameters was seen. Therefore, our results clarify after an increase of AlNNTs in diameter, the HOMO–LUMO energy gaps of tubes have noteworthy increases. Therefore, it is concluded that AlNNTs with smaller diameters can be a better candidate as a sensor for nanodevice applications.

Fig. 5 shows that a comparison of the VIP and VEA of AlNNTs. As seen Table 1, the *VIP* of AlNNTs decreases from 7.58 (for (3,3) AlNNT) to 7.11 eV (for (10,10) AlNNT). However, VIP value of (6,6) AlNNT is slightly higher than that of neighboring AlNNTs (see Fig. 5). The values of VEA remain trapped in the range of 0.78 and 0.87 eV, whereas the (4,4) AlNNT gives a pick, which prefers higher electron affinity. Note that the increasing diameter of AlNNTs does not cause a significant change in VEA.

With increasing the diameter of AlNNTs, the η and ΔN_{tot} of AlNNTs was increased and the ω of the AlNNTs was decreased, which indicated

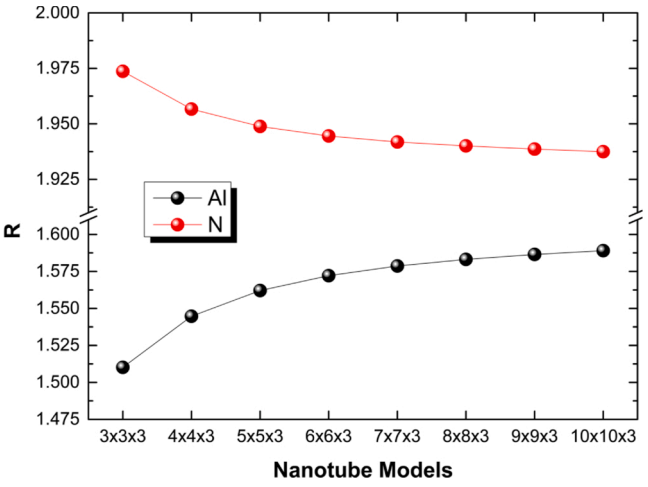

Fig. 7. Order parameters (R) of AlNNT models.

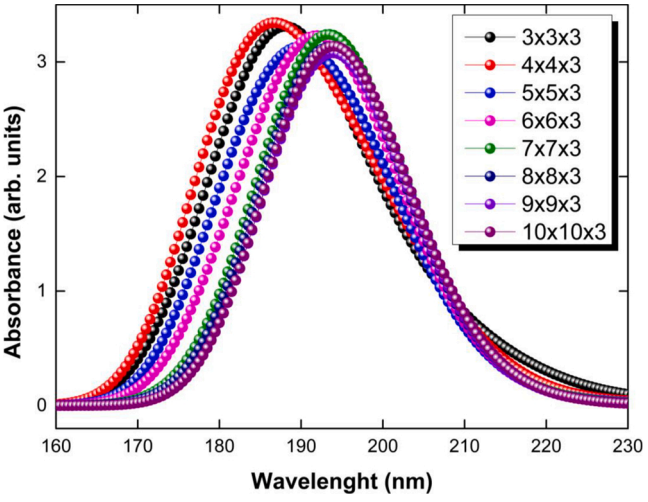

Fig. 8. UV/vis spectra of AlNNT models.

that the chemical reactivity of the AlNNTs was decreased (see Fig. 6). We note that by increasing in chemical hardness for AlNNTs depending on an increase in diameter leads to increase in chemical stability.

In the last part of this section, we calculated segregation phenomena of the different types of atoms with the order parameter (R) to discover

the stable structure of AlNNTs with different diameters (see Fig. 7), which is a desirable property of materials, especially, with high-efficiency. Our results show that a decrease of the *R* of N atoms and an increase of the *R* of Al atoms contribute to the stability of AlNNTs.

Ultraviolet-visible (UV/vis) absorption spectroscopy for the AlNNTs are analyzed by using time-dependent DFT (TD-DFT) and presented in Fig. 8. The maximum UV/vis absorption spectrum values of AlNNTs give an absorption peak located in the UV-C portion of the spectrum, which is good agreement with previous results [42]. Moreover, UV/vis values of (3,3), (4,4), (5,5), (6,6), (7,7), (8,8), (9,9) and (10,10) AlNNTs are found to be 188.0, 186.5, 190.0, 192.0, 193.5, 193.5, 194.0 and 194.0 nm, respectively. Therefore, we note that the UV/vis absorption spectroscopy shifts slightly towards higher wavelengths depending on an increase in diameter.

4. Conclusions

The geometrical structures, energies, electronic properties of armchair (3,3), (4,4), (5,5), (6,6), (7,7), (8,8), (9,9), and (10,10) AlNNTs in different diameter are investigated using DFT calculations. Our results showed that binding energies increases with an increase in diameter of AlNNTs, thus the stability of AlNNTs enhances with increasing diameter. Similarly, increasing chemical hardness for AlNNTs leads to an increase in chemical stability. This also indicates that the chemical reactivity of the AlNNTs was decreased. Depending on the increase in diameter, HOMO-LUMO energy gaps and DOSs show notable changes in the conductivity of AlNNTs. Indeed, the number of Al-N bonds and segregation phenomena of Al and N atoms in the AlNNTs are also indicators of the stability of AlNNTs. Results for UV/vis absorption spectrum of AlNNTs indicate that the maximum wavelength absorption lie in the range 188−194 nm, located in the UV-C region. On the other hand, AlNNTs with smaller diameter has better conditions in terms of conductivity than larger diameter; therefore, they would be preferable as a candidate for the adsorption of the drug or molecule.

CRediT authorship contribution statement

İskender Muz: Conceptualization, Methodology, Software, Validation, Formal analysis, Investigation, Resources, Data curation, Writing - original draft, Writing - review & editing, Visualization, Project administration. **Hasan Kurban:** Formal analysis, Resources, Data curation, Writing - review & editing. **Mustafa Kurban:** Methodology, Software, Validation, Formal analysis, Investigation, Resources, Data curation, Writing - original draft, Writing - review & editing, Supervision.

Declaration of Competing Interest

The authors report no declarations of interest.

Acknowledgments

The numerical calculations reported were partially performed at TUBITAK ULAKBIM, High Performance and Grid Computing Centre (TRUBA resources), Turkey.

References

[1] G. Vijayaraghavan, K.J. Stevenson, Synergistic assembly of dendrimer-templated platinum catalysts on nitrogen-doped carbon nanotube electrodes for oxygen reduction, Langmuir 23 (2007) 5279–5282, https://doi.org/10.1021/la0637263.
[2] S. Lv, L. Ma, X. Shen, H. Tong, One-step copper-catalyzed synthesis of porous carbon nanotubes for high-performance supercapacitors, Microporous Mesoporous Mater. 310 (2021) 110670, https://doi.org/10.1016/j.micromeso.2020.110670.
[3] P. Zhao, P.J. Wang, Z. Zhang, D.S. Liu, Negative differential resistance in a carbon nanotube-based molecular junction, Phys. Lett. A 374 (2010) 1167–1171, https://doi.org/10.1016/j.physleta.2009.12.047.
[4] S.H. Ng, J. Wang, Z.P. Guo, J. Chen, G.X. Wang, H.K. Liu, Single wall carbon nanotube paper as anode for lithium-ion battery, Electrochim. Acta 51 (2005) 23–28, https://doi.org/10.1016/j.electacta.2005.04.045.
[5] H. Mirsalari, A. Maleki, H. Raissi, A. Soltanabadi, Investigation of the pristine and functionalized carbon nanotubes as a delivery system for the anticancer drug dacarbazine: drug encapsulation, J. Pharm. Sci. (2020), https://doi.org/10.1016/j.xphs.2020.10.062.
[6] M. Kurban, İ. Muz, Theoretical investigation of the adsorption behaviors of fluorouracil as an anticancer drug on pristine and B-, Al-, Ga-doped C36 nanotube, J. Mol. Liq. 309 (2020) 113209, https://doi.org/10.1016/j.molliq.2020.113209.
[7] S. Jung, R. Hauert, M. Haluska, C. Roman, C. Hierold, Understanding and improving carbon nanotube-electrode contact in bottom-contacted nanotube gas sensors, Sens. Actuators B Chem. (2020) 129406, https://doi.org/10.1016/j.snb.2020.129406.
[8] S. Wang, Q. Zeng, L. Yang, Z. Zhang, Z. Wang, T. Pei, L. Ding, X. Liang, M. Gao, Y. Li, L.M. Peng, High-performance carbon nanotube light-emitting diodes with asymmetric contacts, Nano Lett. 11 (2011) 23–29, https://doi.org/10.1021/nl101513z.
[9] J.M. Zhang, H.H. Li, Y. Zhang, K.W. Xu, Structural, electronic and magnetic properties of the 3d transition-metal-doped AlN nanotubes, Phys. E Low-Dimens. Syst. Nanostruct. 43 (2011) 1249–1254, https://doi.org/10.1016/j.physe.2011.02.009.
[10] G. Wang, H. Yuan, A. Kuang, W. Hu, G. Zhang, H. Chen, High-capacity hydrogen storage in Li-decorated (AlN)n (n = 12, 24, 36) nanocages, Int. J. Hydrogen Energy 39 (2014) 3780–3789, https://doi.org/10.1016/j.ijhydene.2013.12.138.
[11] H. Anaraki-Ardakani, A computational study on the application of AlN nanotubes in Li-ion batteries, Phys. Lett. Sect. A Gen. At. Solid State Phys. 381 (2017) 1041–1046, https://doi.org/10.1016/j.physleta.2017.01.010.
[12] A. Ahmadi, N.L. Hadipour, M. Kamfiroozi, Z. Bagheri, Theoretical study of aluminum nitride nanotubes for chemical sensing of formaldehyde, Sens. Actuators B: Chem. 161 (2012) 1025–1029, https://doi.org/10.1016/j.snb.2011.12.001.
[13] M. Noei, A.A. Salari, N. Ahmadaghaei, Z. Bagheri, A.A. Peyghan, DFT study of the dissociative adsorption of HF on an AlN nanotube, C. R. Chim. 16 (2013) 985–989, https://doi.org/10.1016/j.crci.2013.05.007.
[14] J. Beheshtian, Z. Bagheri, M. Kamfiroozi, A. Ahmadi, A theoretical study of CO adsorption on aluminum nitride nanotubes, Struct. Chem. 23 (2012) 653–657, https://doi.org/10.1007/s11224-011-9911-z.
[15] M. Noei, M. Ebrahimikia, Y. Saghapour, M. Khodaverdi, A.A. Salari, N. Ahmadaghaei, Removal of ethyl acetylene toxic gas from environmental systems using AlN nanotube, J. Nanostruct. Chem. 5 (2015) 213–217, https://doi.org/10.1007/s40097-015-0152-3.
[16] İ. Muz, M. Kurban, A comprehensive study on electronic structure and optical properties of carbon nanotubes with doped B, Al, Ga, Si, Ge, N, P and As and different diameters, J. Alloys Compd. 802 (2019) 25–35, https://doi.org/10.1016/j.jallcom.2019.06.210.
[17] I. Muz, M. Kurban, Electronic transport and non-linear optical properties of hexathiopentacene (HTP) nanorings: a DFT study, J. Electron. Mater. 49 (2020) 3282–3289, https://doi.org/10.1007/s11664-020-08017-w.
[18] İ. Muz, F. Göktaş, M. Kurban, Size dependence in the electronic and optical properties of a BN analogue of two-dimensional graphdiyne: a theoretical study, Chem. Phys. 539 (2020), https://doi.org/10.1016/j.chemphys.2020.110929.
[19] H. Kurban, M. Kurban, M. Dalkılıç, Density-functional tight-binding approach for the structural analysis and electronic structure of copper hydride metallic nanoparticles, Mater. Today Commun. 21 (2019) 100648, https://doi.org/10.1016/j.mtcomm.2019.100648.
[20] Y. Li, R. Ahuja, J.A. Larsson, Communication: origin of the difference between carbon nanotube armchair and zigzag ends, J. Chem. Phys. 140 (2014), https://doi.org/10.1063/1.4867744.
[21] M.J. Frisch, G.W. Trucks, H.B. Schlegel, G.E. Scuseria, M.A. Robb, J.R. Cheeseman, G. Scalmani, V. Barone, B. Mennucci, G.A. Petersson, H. Nakatsuji, M. Caricato, X. Li, H.P. Hratchian, A.F. Izmaylov, J. Bloino, G. Zheng, J.L. Sonnenberg, M. Hada, M. Ehara, K. Toyota, R. Fukuda, J. Hasegawa, M. Ishida, T. Nakajima, Y. Honda, O. Kitao, H. Nakai, T. Vreven, J.A. Montgomery, J.E. Peralta, F. Ogliaro, M. Bearpark, J.J. Heyd, E. Brothers, K.N. Kudin, V.N. Staroverov, R. Kobayashi, J. Normand, K. Raghavachari, A. Rendell, J.C. Burant, S.S. Iyengar, J. Tomasi, M. Cossi, N. Rega, J.M. Millam, M. Klene, J.E. Knox, J.B. Cross, V. Bakken, C. Adamo, J. Jaramillo, R. Gomperts, R.E. Stratmann, O. Yazyev, A.J. Austin, R. Cammi, C. Pomelli, J.W. Ochterski, R.L. Martin, K. Morokuma, V.G. Zakrzewski, G.A. Voth, P. Salvador, J.J. Dannenberg, S. Dapprich, A.D. Daniels, Farkas, J. B. Foresman, J.V. Ortiz, J. Cioslowski, D.J. Fox, Gaussian 09., Revision E.01.01, Gaussian Inc., Wallingford C.T, 2009.
[22] A.D. Becke, A new mixing of hatree-fock and local density functional theories, J. Chem. Phys. 98 (1993) 1372–1377, https://doi.org/10.1063/1.464304.
[23] S. Grimme, S. Ehrlich, L. Goerigk, Effect of the damping function in dispersion corrected density functional theory, J. Comput. Chem. 32 (2011) 1456–1465, https://doi.org/10.1002/jcc.21759.
[24] T. Yanai, D.P. Tew, N.C. Handy, A new hybrid exchange–correlation functional using the Coulomb-attenuating method (CAM-B3LYP), Chem. Phys. Lett. 393 (2004) 51–57, https://doi.org/10.1016/j.cplett.2004.06.011.
[25] B.M. Wong, T.H. Hsieh, Optoelectronic and excitonic properties of oligoacenes: substantial improvements from range-separated time-dependent density functional theory, J. Chem. Theory Comput. 6 (2010) 3704–3712, https://doi.org/10.1021/ct100529s.
[26] A.E. Raeber, B.M. Wong, The importance of short- and long-range exchange on various excited state properties of DNA monomers, stacked complexes, and watson-

crick pairs, J. Chem. Theory Comput. 11 (2015) 2199–2209, https://doi.org/10.1021/acs.jctc.5b00105.
[27] M. Kurban, B. Gündüz, F. Göktaş, Experimental and theoretical studies of the structural, electronic and optical properties of BCzVB organic material, Optik (Stuttg.) 182 (2019) 611–617, https://doi.org/10.1016/j.ijleo.2019.01.080.
[28] İ. Muz, M. Kurban, The electronic structure, transport and structural properties of nitrogen-decorated graphdiyne nanomaterials, J. Alloys Compd. 842 (2020), https://doi.org/10.1016/j.jallcom.2020.155983.
[29] N.M. O'Boyle, A.L. Tenderholt, K.M. Langner, cclib: a library for package-independent computational chemistry algorithms, J. Comput. Chem. 29 (2008) 839–845, https://doi.org/10.1002/jcc.20823.
[30] T. Koopmans, Über die Zuordnung von Wellenfunktionen und Eigenwerten zu den Einzelnen Elektronen Eines Atoms, Physica 1 (1934) 104–113, https://doi.org/10.1016/S0031-8914(34)90011-2.
[31] R.G. Parr, R.G. Pearson, Absolute hardness—companion parameter to absolute electronegativity, J. Am. Chem. Soc. 105 (1983) 7512–7516, https://doi.org/10.1021/ja00364a005.
[32] X. Wu, Z. Wei, Q. Liu, T. Pang, G. Wu, Structure and bonding in quaternary [Formula presented] clusters, J. Alloys Compd. 687 (2016) 115–120, https://doi.org/10.1016/j.jallcom.2016.06.117.
[33] K.P. Huber, G. Herzberg, Molecular Spectra and Molecular Structure, Springer US, 1979, https://doi.org/10.1007/978-1-4757-0961-2.
[34] H. Kurban, M. Dalkilic, S. Temiz, M. Kurban, Tailoring the structural properties and electronic structure of anatase, brookite and rutile phase TiO2 nanoparticles: DFTB calculations, Comput. Mater. Sci. 183 (2020) 109843, https://doi.org/10.1016/j.commatsci.2020.109843.
[35] M.T. Baei, F. Kaveh, P. Torabi, S.Z. Sayyad-Alangi, Adsorption properties of oxygen on H-capped (5, 5) boron nitride nanotube (BNNT)-a density functional theory, E-J. Chem. 8 (2011) 609–614, https://doi.org/10.1155/2011/912894.
[36] J.K. Burdett, B.A. Coddens, G.V. Kulkarni, Band gap and stability of solids, Inorg. Chem. 27 (1988) 3259–3261, https://doi.org/10.1021/ic00291a050.
[37] A. Hosseinian, E. Vessally, A. Bekhradnia, K. Nejati, G. Rahimpour, Benzoylethanamine drug interaction with the AlN nanosheet, nanotube and nanocage: density functional theory studies, Thin Solid Films 640 (2017) 93–98, https://doi.org/10.1016/j.tsf.2017.08.049.
[38] J.M. de Almeida, T. Kar, P. Piquini, AlN, GaN, AlxGa1 - xN nanotubes and GaN/AlxGa1 - xN nanotube heterojunctions, Phys. Lett. Sect. A Gen. At. Solid State Phys. 374 (2010) 877–881, https://doi.org/10.1016/j.physleta.2009.11.084.
[39] P. Sripadung, N. Nunthaboot, B. Wanno, Group 8B transition metal-doped (5,5) boron nitride nanotubes for NH3 storage and sensing: a theoretical investigation, Monatshefte Fur Chem. 150 (2019) 1011–1018, https://doi.org/10.1007/s00706-019-02403-9.
[40] M.T. Baei, S. Hashemian, P. Torabi, A. Gharehbaghi, Electronic structure study of gallium and indium doped (4,4) armchair single-walled boron nitride nanotubes for production of solid-state devices, Fullerenes Nanotubes Carbon Nanostruct. 23 (2015) 68–77, https://doi.org/10.1080/1536383X.2012.758109.
[41] M.T. Baei, Y. Kanani, V.J. Rezaei, A. Soltani, Adsorption phenomena of gas molecules upon Ga-doped BN nanotubes: a DFT study, Appl. Surf. Sci. 295 (2014) 18–25, https://doi.org/10.1016/j.apsusc.2013.12.136.
[42] A. Soltani, A. Sousaraei, M. Mirarab, H. Balakheyli, Interaction of CNCl molecule and single-walled AlN nanotubes using DFT and TD-DFT calculations, J. Saudi Chem. Soc. 21 (2017) 270–276, https://doi.org/10.1016/j.jscs.2015.06.006.